

Compact Configuration Evaluation - Mosaicing

Melvyn Wright

Radio Astronomy laboratory, University of California, Berkeley, CA, 94720

ABSTRACT

In this memo, we compare the mosaicing performance of compact configurations. MIRIAD scripts simulate mosaic observations with ALMA, calculate error images and pipeline the results into tables. The residual imaging errors are characterized by the recovered flux, peak flux density and the sidelobe levels. We present tables of the sidelobe levels and image fidelity for source declinations from +60 to -60 degrees. Mosaic images for source diameters 24", and 32" are analyzed. For the 24" source, a Gaussian configuration provides the best image fidelity. For the 32" source, the most compact configuration provides better sampling of the large scale structure and better image fidelity, except at high declinations where the array is strongly shadowed.

1. Introduction

Three compact antenna configurations are being considered for ALMA: 1) a compact array for maximum brightness sensitivity. At high declinations this array has many shadowed antennas and an elongated beam. 2) a Gaussian array with ~ 1.5 times the resolution, and 3) a N-S extended array with a circular beam and the same resolution as configuration 1 for declination 30 deg sources.

Single field imaging for these three configurations was analyzed in ALMA memo 428. In this memo we evaluate the mosaicing performance for the same 24" and 32" diameter source models used in memo 428. The original 3 configurations have been revised to reduce the number of stations needed and to reduce the shadowing. Mosaic images were made for all six configurations.

The purpose of this memo is to compare the performance of the compact configurations for mosaicing. The most serious defect is the lack of baselines shorter than the 12m antenna diameter. In this memo we discuss mosaic observations using single dish images to complement the missing short interferometer spacings.

2. The imaging procedure

The imaging procedures are simple **unix csh** scripts which control **MIRIAD** tasks. The mosaicing script makes simulated uv-data and single dish data using a VLA image of Cas A as a model. The

model is scaled to various source sizes. Thermal noise, appropriate for ALMA is added to the uv-data. The uv-data is Fourier transformed to make images and deconvolved using Maximum Entropy (MEM) algorithms. An error image is formed by subtracting the original image model convolved to the same resolution by the Gaussian restoring beam. A control script invokes the mosaicing script for a selected range of source models, declinations and array configurations. A number of other parameters such as the uv-sample interval and mosaic pointing pattern were also varied to assess the behaviour of the simulated images. The mosaicing process, the simulated images and the residual images are displayed on the terminal, and saved on disk for further analysis. The numerical results are accumulated into a table. The script was run on a Sun ultra 10 with 250 kB of memory. Timing statistics were kept for each step. For 7- to 19-pointing mosaics with $\sim 350,000$ uv samples, each simulation takes $\sim 6 - 10$ min. The procedure is simple enough and fast enough that an inexperienced ALMA user could explore the outcome of proposed or actual observations for a given source model and data sampling.

2.1. The Source Model

We used the same scaled Cas A source models as in memo 428, but doubled the size of the image to accomodate the convolution by the $24''$ primary beam for the single dish image. This is necessary to avoid an unphysical edge to the single dish image and is an important point to remember when observing. A single dish image is the real source brightness distribution convolved by the single dish beam. Any emission outside the image frame is convolved into the field of view and may be aliased into the image in the mosaicing process. For sources which are not isolated in space or in velocity, one may need to image a larger region to avoid aliasing into the field of interest. We filled out the double size model image with zeros outside the original VLA 1024×1024 image. After convolution by a $24''$ primary beam, the single dish image falls to 0.5% at the edges of the 2048×2048 image.

2.2. Sampling

The Nyquist sample interval for the pointing centers, $\delta\theta = \lambda/2D$ where D is the antenna diameter. The number of pointings, $N_p = \Omega/(\lambda/2D)^2$, where Ω is the source solid angle. For the 12m ALMA antenna at 230 GHz $\delta\theta = 10.8''$. We require many pointing centers to image even a rather modest size source; we used hexagonal patterns of 7- and 19-pointings for source diameters of $24''$ and $32''$ in this study.

The Nyquist interval for the uv data, $\delta uv = D/2\lambda$. For mosaic observations we should sample uv data for each pointing at the Nyquist rate. This leads a sampling rate = $baseline/(D/2) \times N_p \times sdot$ s^{-1} , where $sdot = 7.27 \cdot 10^{-5} s^{-1}$. The Nyquist sample interval $\sim 30-80$ s for 7- to 19-pointing mosaics and the maximum baselines in these configurations.

The source model is multiplied by the primary beam pattern at each pointing. uv data were generated for the given pointing pattern and sample intervals with random noise corresponding to a system temperature 40 K, and a bandwidth 8 GHz. Each configuration was sampled from HA -1 to $+1$ hours which gives a well sampled uv -coverage for these configurations. Since we wish to study the ability of the compact configurations to image the source we have not added any pointing or primary beam errors to either the uv data or to the single dish data, as these would dilute the differences between the configurations.

2.3. Imaging

We made mosaic images for source sizes $24''$ and $32''$ at 230 GHz and investigated the ability of the 3 compact configurations to image these structures. We used the mosaicing option in Miriad’s imaging task which combines the uv data from multiple pointings into a mosaic image (Sault, Staveley-Smith & Brouw, 1996; ”Miriad Users Guide”, Bob Sault & Neil Killeen, 1999; Holdaway 1999). We discarded all shadowed data (see memo 428).

The images were deconvolved with the MEM algorithm using the single dish image as a default image. In practice the image fidelity is likely to be limited by the single dish data and a joint deconvolution of the interferometer and single dish data may be used. The extent to which the single dish data can be deconvolved will be limited by our characterization of the primary beam and pointing errors in the single dish data, and also by thermal noise and systematic residual errors such as ground pickup or atmospheric fluctuations. Since we wish to investigate the differences between the compact configurations we did not add any errors to the single dish data and did not deconvolve the single dish image. The Miriad MEM algorithm converts the single dish image to Jy/pixel units and uses the single dish data to constrain both the total flux and the spatial frequencies unsampled by the interferometer data.

3. Results

In Table 1 & 2 we characterize the mosaicing performance by the total flux, peak flux density, and residuals in the difference between the synthesised image and the original model convolved to the same resolution. The image fidelity is listed in the last column as the ratio of the peak flux density to the on-source RMS on the residual image. The RMS was evaluated in a standard bounding box $1.25 \times$ the image diameter. The deconvolution and image fidelity might be improved by using more a-priori information, or information about the source structure revealed by the imaging process, but in this memo we are focussed on the differences between the compact configurations. The image fidelity is expected to be much smaller in practice when pointing and primary beam errors are taken into account (Cornwell, Holdaway, & Uson, 1993). The tables are given for reference. The total flux density in the original model image is 732 Jy. The thermal noise, $\sim 6\text{--}12 \mu\text{Jy}$ for these 7- and 19-pointing mosaiced images with an 8 GHz bandwidth at 230 GHz, is insignificant compared

with the imaging errors. The compact configurations are compared in a number of graphs.

3.1. Comparisons in the Image domain

Figure 1 shows the synthesised image and Maximum Entropy deconvolution of the $32''$ source model imaged with the original compact configuration 2 at declination -30 deg. The synthesised image [upper panel] combines all the pointings in a linear mosaic; the spatial filtering of the large scale structure is readily apparent. The deconvolved image [lower panel] includes the single dish data and has recovered most of the large scale structure. Figure 2 shows the residual image. The peak residuals in the corners suggest that the deconvolution could be further improved by using a bounding box which was a better match to the source structure. The residuals from the mosaiced observation are $\sim 10\times$ lower than a single field observation with the same source model and antenna configuration (see memo 428 figure 3).

Figures 3 and 4 plot the image fidelity for the original and revised configurations as a function of the source declination. For the $24''$ source, the Gaussian configurations provide the best image fidelity at all declinations. For the $32''$ source, the most compact configuration 1 provides better sampling of the large scale structure and better image fidelity, except at high declinations where the array is strongly shadowed. For the larger source, configurations 2 and 3 provide better image fidelity at high declinations. The revised, stretched configuration 3 is now highly specialized for high declinations, and gives much poorer image fidelity between declinations -50 to $+10$.

3.2. Comparisons in the Fourier domain

To see the effects of the uv-sampling, we also compare the configurations in the Fourier domain. A radial distribution of the Fourier transform for the deconvolved and residual images shows most of the germane points for this almost circular source model.

Figures 5 and 6 plot the Fourier transforms for a $32''$ source at declinations of -30 and $+30$ degrees. The solid black line shows the input model. The upper broken lines plot the Fourier transforms of the MEM images, before convolving by a restoring beam. The radial distributions are plotted over the range of uv-spacings sampled by the 3 configurations, and follow the model structure quite well except at the highest spatial frequencies which are not sampled uniformly in all directions. The break away from the input model occurs at the largest uv-distance which has good azimuthal sampling. Part of the benefits of one or another configuration are the range of spatial frequencies over which there is good fidelity. The most compact configuration 1 samples a smaller range of uv-spacings than configurations 2 and 3. The 3 lower curves show the difference images between the MEM images and the original model image, both convolved by the restoring beam. The image fidelity at different spatial frequencies is measured by the vertical distance from the model image. The image fidelity of the mosaiced images is $\sim 10 \times$ larger than for single field images with the

same source size and antenna configuration (see memo 428 figure 4). The fidelity degrades at high spatial frequencies where the uv sampling is azimuthally incomplete for each configuration, and in the hump at $3.9 - 4 \text{ k}\lambda$ (the inverse of Darrel’s Dip), which lies between the shortest interferometer spacing and the single dish data. The hump is less pronounced at declination $+30$ where the shortest interferometer spacings are projected to 12m, whereas at declination -30 the shortest interferometer spacings are \sim the minimum antenna spacing of 15m. Configuration 1 gives the best image fidelity at declination -30 ; Configuration 3 gives the best image fidelity at declination $+30$ for a $32''$ source.

3.3. Mosaic sample interval

Figure 7 shows the degradation in image fidelity for various mosaic sampling patterns as the pointing sample interval is increased away from the Nyquist interval. Each pointing pattern is a hexagonal mosaic with the same center using the $32''$ source model and the original 3 compact configurations. A hexagonal pattern provides a convenient pattern for sampling an arbitrary shaped source. In principal with a hexagonal pattern the Nyquist interval $\lambda/2D$, is oversampled by a factor $2/\sqrt{3}$, but in practice this provides good overlap of the pointing positions and there is no loss in sensitivity. Pattern 1 is a 19-pointing mosaic with $10.8''$ spacing, pattern 2 is a 19-pointing mosaic with $12''$ spacing. For a $32''$ source diameter the 19-pointing mosaic give more complete coverage of the source. For configuration 1, the $12''$ spacing gives somewhat better fidelity. Pattern 3 is a 7-pointing mosaic with $15''$ spacing, pattern 4 is a 7-pointing mosaic with $12''$ spacing, pattern 5 is a 7-pointing mosaic with $20''$ spacing. If a 7-pointing mosaic is used, the $15''$ spacing gives the best coverage of the source; the $12''$ spacing is closer to the Nyquist interval, but has poor coverage of the edges of the source, whilst the $20''$ spacing is \sim twice the Nyquist interval, but covers the source better. Undersampling the pointing for mosaiced images degraded the image fidelity, although this might be suitable way to survey a large area of sky with a sparse distribution of sources.

3.4. uv data sample interval

Figure 7 shows the degradation in image fidelity as the uv sample interval is increased away from the Nyquist interval. Some combinations of antenna configuration and source declination are more sensitive than others to an increased uv sample interval. For the compact configurations the sampling rate is quite modest; the uv data can be sampled at the Nyquist rate except perhaps for very large mosaics. For more extended antenna configurations and large mosaics the Nyquist sampling rate is more challenging.

4. Conclusions

For the 24'' source, the Gaussian configurations provide the best image fidelity. For the 32'' source, the most compact configuration 1 provides better sampling of the large scale structure and better image fidelity, except at high declinations where the array is strongly shadowed. The image fidelity of the mosaiced images is up to $\sim 10 \times$ larger than for single field images with the same source size and antenna configuration. For the larger source, configurations 2 and 3 provide better image fidelity at high declinations. The revised, stretched configuration 3 is now highly specialized for high declinations, and gives much poorer image fidelity between declinations -50 to $+10$. The image fidelity degrades slowly as the pointing or uv sample interval is increased away from the Nyquist intervals.

5. References

- "Image Fidelity", M.C.H. Wright, 1999, BIMA memo 73, <http://bima.astro.umd.edu/memo/memo.html>
- "An approach to interferometric mosaicing", Sault, R.J., Staveley-Smith, L & Brouw, W.N., 1996, A&A Supp., 120, 375
- "Miriad Users Guide", 1999, Bob Sault & Neil Killeen, <http://www.atnf.csiro.au/computing/software/miriad>
- "Mosaicing with Interferometer Arrays", Holdaway. M.A., 1999, ASP Conference series 180, 401.
- "Radio-interferometric imaging of very large objects: implications for array design", Cornwell, T.J., Holdaway, M.A. & Uson, J.M., 1993, A&A 271, 697.

Table 1a: Original configurations: Mosaic Imaging with single dish data – Source size $\sim 24''$

Config	DEC	Beam[$''$]	Model Peak[Jy]	Image Flux	Peak	RMS	Max	Min	Fidelity
config1	60	18.70 x 1.85	65.3	650.2	58.5	2.427	5.586	-13.143	24
config2	60	6.72 x 0.96	23.3	742.2	23.1	0.188	0.623	-0.877	123
config3	60	9.56 x 1.46	40.8	721.6	39.7	0.450	1.054	-3.060	88
config1	45	5.68 x 1.57	33.0	748.7	31.8	0.516	2.328	-0.854	62
config2	45	2.63 x 1.00	12.6	743.6	12.6	0.026	0.128	-0.079	485
config3	45	2.21 x 1.55	16.2	740.1	16.0	0.030	0.137	-0.158	534
config1	30	2.56 x 1.59	18.5	738.2	18.3	0.043	0.200	-0.174	427
config2	30	1.90 x 1.09	10.6	742.4	10.7	0.015	0.071	-0.055	710
config3	30	1.60 x 1.39	11.6	740.1	11.5	0.017	0.073	-0.092	677
config1	15	2.17 x 1.67	17.0	736.3	16.8	0.029	0.124	-0.170	580
config2	15	1.61 x 1.25	10.6	739.4	10.6	0.011	0.054	-0.059	961
config3	15	1.69 x 1.11	10.1	740.3	10.1	0.013	0.067	-0.093	779
config1	0	1.83 x 1.70	15.1	739.5	14.9	0.026	0.104	-0.144	574
config2	0	1.38 x 1.28	9.6	742.6	9.5	0.011	0.042	-0.055	867
config3	0	1.73 x 0.94	9.0	741.7	9.0	0.011	0.057	-0.071	818
config1	-15	1.70 x 1.70	14.3	739.8	14.2	0.024	0.089	-0.138	592
config2	-15	1.28 x 1.28	9.0	742.2	9.0	0.009	0.035	-0.051	997
config3	-15	1.74 x 0.87	8.5	743.3	8.5	0.010	0.055	-0.083	848
config1	-30	1.70 x 1.69	14.2	739.0	14.2	0.023	0.086	-0.114	616
config2	-30	1.28 x 1.27	8.9	743.6	8.9	0.010	0.036	-0.068	894
config3	-30	1.74 x 0.87	8.5	742.6	8.4	0.010	0.057	-0.075	844
config1	-45	1.81 x 1.70	15.0	739.6	14.8	0.025	0.100	-0.144	592
config2	-45	1.36 x 1.28	9.4	742.7	9.4	0.011	0.038	-0.052	859
config3	-45	1.73 x 0.93	8.9	743.3	8.9	0.011	0.057	-0.086	811
config1	-60	2.10 x 1.68	16.7	736.5	16.5	0.028	0.124	-0.167	589
config2	-60	1.58 x 1.26	10.5	739.5	10.5	0.010	0.049	-0.060	1046
config3	-60	1.70 x 1.09	10.0	741.9	10.0	0.013	0.059	-0.116	771

Table 1b: Original configurations: Mosaic Imaging with single dish data – Source size $\sim 32''$

Config	DEC	Beam[$''$]	Model Peak[Jy]	Image Flux	Peak	RMS	Max	Min	Fidelity
config1	60	17.81 x 1.86	44.8	650.8	40.8	0.964	1.634	-5.567	42
config2	60	6.38 x 0.97	14.5	752.4	14.3	0.130	0.426	-0.231	110
config3	60	9.22 x 1.50	27.5	736.9	26.7	0.335	2.763	-0.603	80
config1	45	5.69 x 1.58	21.0	764.5	20.3	0.577	1.381	-1.044	35
config2	45	2.62 x 1.01	7.9	750.4	7.8	0.024	0.070	-0.047	324
config3	45	2.20 x 1.56	10.2	753.1	10.1	0.024	0.072	-0.089	422
config1	30	2.53 x 1.60	11.6	759.0	11.7	0.036	0.115	-0.175	324
config2	30	1.89 x 1.10	6.6	759.1	6.6	0.018	0.057	-0.046	367
config3	30	1.61 x 1.38	7.2	751.3	7.2	0.016	0.047	-0.055	448
config1	15	2.17 x 1.68	10.7	745.9	10.7	0.018	0.057	-0.075	593
config2	15	1.61 x 1.25	6.5	759.0	6.5	0.014	0.043	-0.054	467
config3	15	1.70 x 1.11	6.3	750.9	6.2	0.011	0.035	-0.038	566
config1	0	1.83 x 1.70	9.5	740.5	9.4	0.014	0.055	-0.053	672
config2	0	1.38 x 1.28	5.9	756.0	5.9	0.011	0.036	-0.027	533
config3	0	1.73 x 0.94	5.5	753.5	5.6	0.012	0.037	-0.036	464
config1	-15	1.70 x 1.70	8.9	739.6	8.9	0.017	0.051	-0.067	523
config2	-15	1.28 x 1.28	5.5	753.9	5.5	0.013	0.037	-0.033	425
config3	-15	1.75 x 0.88	5.3	750.1	5.2	0.013	0.030	-0.034	402
config1	-30	1.70 x 1.69	8.9	737.6	8.8	0.017	0.050	-0.064	520
config2	-30	1.28 x 1.27	5.5	750.6	5.5	0.012	0.033	-0.032	457
config3	-30	1.75 x 0.87	5.2	746.9	5.2	0.012	0.029	-0.037	434
config1	-45	1.81 x 1.70	9.4	739.7	9.3	0.014	0.054	-0.051	665
config2	-45	1.36 x 1.28	5.8	755.5	5.8	0.011	0.036	-0.026	528
config3	-45	1.73 x 0.93	5.5	750.7	5.5	0.011	0.032	-0.032	500
config1	-60	2.10 x 1.69	10.5	745.4	10.4	0.017	0.056	-0.071	615
config2	-60	1.57 x 1.26	6.4	758.3	6.5	0.013	0.041	-0.049	497
config3	-60	1.70 x 1.09	6.2	750.8	6.2	0.012	0.036	-0.037	513

Table 2a: Revised configurations: Mosaic Imaging with single dish data – Source size $\sim 24''$

Config	DEC	Beam[$''$]	Model Peak[Jy]	Image Flux	Peak	RMS	Max	Min	Fidelity
config1	60	13.75 x 1.71	54.3	690.9	50.1	1.361	2.562	-7.261	37
config2	60	6.99 x 0.93	23.5	750.9	23.1	0.281	2.441	-0.537	82
config3	60	5.20 x 1.28	25.9	746.5	25.4	0.149	1.194	-0.703	171
config1	45	3.35 x 1.68	23.7	747.7	23.3	0.171	0.598	-0.452	136
config2	45	2.40 x 1.07	12.5	742.5	12.4	0.023	0.116	-0.068	540
config3	45	1.96 x 1.44	13.9	740.1	13.9	0.021	0.095	-0.112	662
config1	30	2.47 x 1.68	18.8	738.7	18.6	0.040	0.192	-0.214	464
config2	30	1.81 x 1.18	11.0	740.1	11.0	0.012	0.069	-0.047	917
config3	30	1.53 x 1.41	11.3	739.1	11.3	0.012	0.056	-0.082	940
config1	15	1.94 x 1.63	15.3	738.3	15.2	0.025	0.105	-0.175	607
config2	15	1.45 x 1.27	9.9	741.0	9.9	0.011	0.044	-0.051	900
config3	15	1.51 x 1.12	9.3	742.3	9.3	0.013	0.052	-0.077	715
config1	0	1.66 x 1.64	13.6	740.7	13.5	0.022	0.098	-0.151	615
config2	0	1.29 x 1.26	8.9	741.6	8.9	0.009	0.045	-0.044	992
config3	0	1.50 x 0.96	8.1	740.0	8.1	0.022	0.080	-0.108	370
config1	-15	1.64 x 1.54	12.9	737.9	12.7	0.018	0.080	-0.108	707
config2	-15	1.29 x 1.17	8.4	742.6	8.4	0.008	0.039	-0.071	1050
config3	-15	1.50 x 0.90	7.7	735.3	7.7	0.027	0.108	-0.138	284
config1	-30	1.64 x 1.54	12.9	736.6	12.6	0.017	0.080	-0.079	742
config2	-30	1.29 x 1.16	8.4	742.6	8.4	0.008	0.036	-0.060	1048
config3	-30	1.50 x 0.89	7.6	732.1	7.6	0.025	0.071	-0.126	305
config1	-45	1.64 x 1.64	13.5	740.9	13.4	0.022	0.090	-0.150	610
config2	-45	1.29 x 1.24	8.8	744.0	8.9	0.010	0.041	-0.066	886
config3	-45	1.50 x 0.95	8.1	733.9	8.1	0.018	0.044	-0.110	448
config1	-60	1.90 x 1.64	15.1	738.2	15.0	0.025	0.106	-0.174	601
config2	-60	1.44 x 1.29	10.0	740.5	9.9	0.010	0.042	-0.052	993
config3	-60	1.50 x 1.11	9.2	742.6	9.2	0.012	0.054	-0.073	763

Table 2b: Revised configurations: Mosaic Imaging with single dish data – Source size $\sim 32''$

Config	DEC	Beam[$''$]	Model Peak[Jy]	Image Flux	Peak	RMS	Max	Min	Fidelity
config1	60	13.22 x 1.72	37.1	698.3	34.7	0.757	2.361	-1.651	46
config2	60	6.72 x 0.93	14.5	750.2	14.3	0.182	0.630	-0.393	79
config3	60	5.15 x 1.28	16.0	750.8	16.0	0.090	0.288	-0.168	178
config1	45	3.36 x 1.68	15.0	762.4	14.4	0.239	0.654	-0.506	60
config2	45	2.39 x 1.07	7.8	748.6	7.7	0.029	0.077	-0.065	266
config3	45	1.96 x 1.46	8.8	751.4	8.7	0.018	0.057	-0.067	486
config1	30	2.45 x 1.69	11.9	753.0	11.9	0.029	0.090	-0.109	409
config2	30	1.81 x 1.18	6.8	759.4	6.8	0.013	0.043	-0.034	526
config3	30	1.53 x 1.41	7.0	757.2	7.0	0.014	0.046	-0.054	499
config1	15	1.94 x 1.64	9.6	746.2	9.6	0.016	0.052	-0.057	599
config2	15	1.45 x 1.28	6.1	757.6	6.1	0.012	0.041	-0.033	512
config3	15	1.51 x 1.12	5.7	730.6	5.7	0.012	0.058	-0.066	473
config1	0	1.66 x 1.64	8.5	740.1	8.4	0.015	0.044	-0.051	563
config2	0	1.30 x 1.25	5.5	752.8	5.5	0.013	0.038	-0.035	423
config3	0	1.51 x 0.96	5.0	697.5	4.9	0.025	0.107	-0.082	197
config1	-15	1.64 x 1.54	8.0	731.8	7.9	0.019	0.062	-0.070	418
config2	-15	1.30 x 1.17	5.2	752.5	5.2	0.017	0.037	-0.044	304
config3	-15	1.50 x 0.90	4.7	662.6	4.6	0.039	0.179	-0.114	117
config1	-30	1.64 x 1.54	8.0	733.9	7.9	0.021	0.069	-0.071	377
config2	-30	1.30 x 1.16	5.1	753.1	5.2	0.017	0.037	-0.044	303
config3	-30	1.50 x 0.89	4.6	656.9	4.6	0.041	0.191	-0.125	111
config1	-45	1.64 x 1.64	8.4	740.2	8.4	0.016	0.044	-0.053	523
config2	-45	1.30 x 1.24	5.4	755.8	5.4	0.013	0.036	-0.026	419
config3	-45	1.50 x 0.96	4.9	685.2	4.9	0.027	0.117	-0.079	180
config1	-60	1.90 x 1.65	9.5	746.1	9.5	0.016	0.051	-0.061	593
config2	-60	1.44 x 1.29	6.1	757.2	6.2	0.012	0.041	-0.034	513
config3	-60	1.50 x 1.11	5.6	721.3	5.6	0.011	0.030	-0.050	507

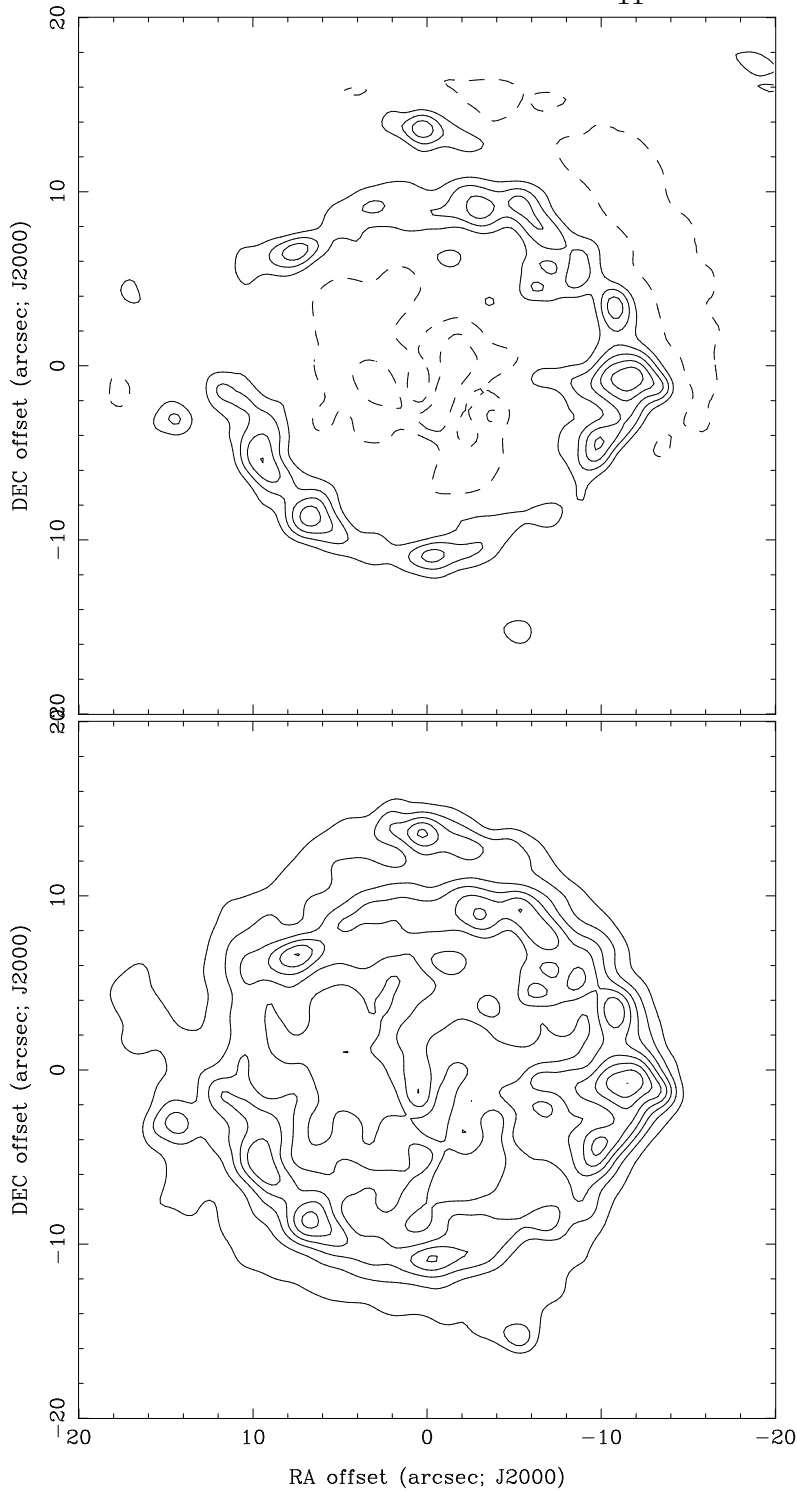


Fig. 1.— Mosaic Image [upper panel] and Maximum Entropy deconvolution [lower panel] 1/10 full scale, imaged with the original compact configuration 2 at declination -30 deg. Contours at 12.5 % of peak.

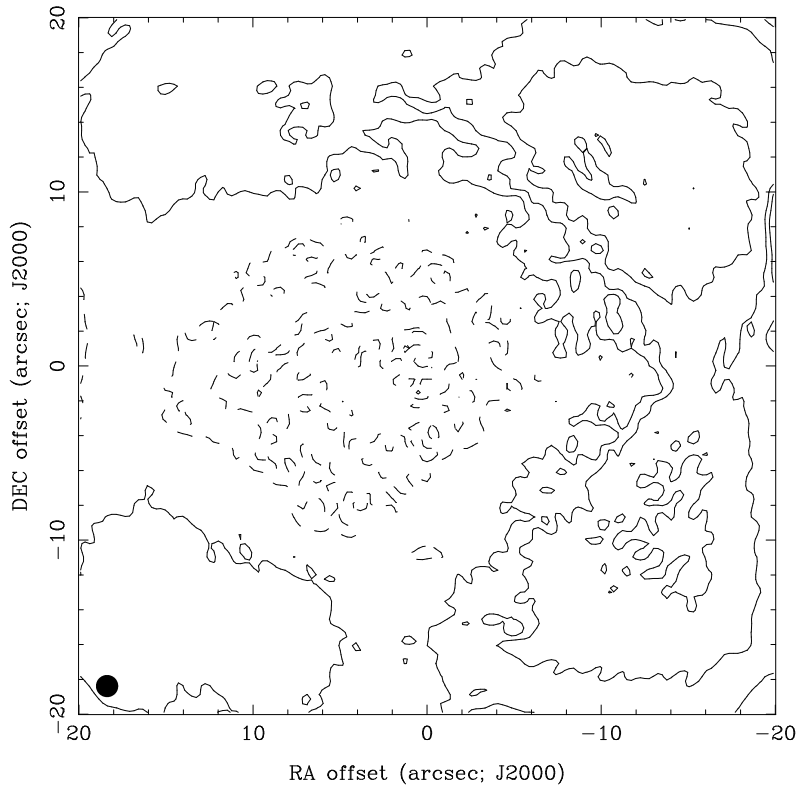


Fig. 2.— Residual Image for the original configuration 2 at declination -30 deg. Contours at 0.14 % of Maximum Entropy Image peak. The synthesised beam FWHM is indicated in the lower left corner.

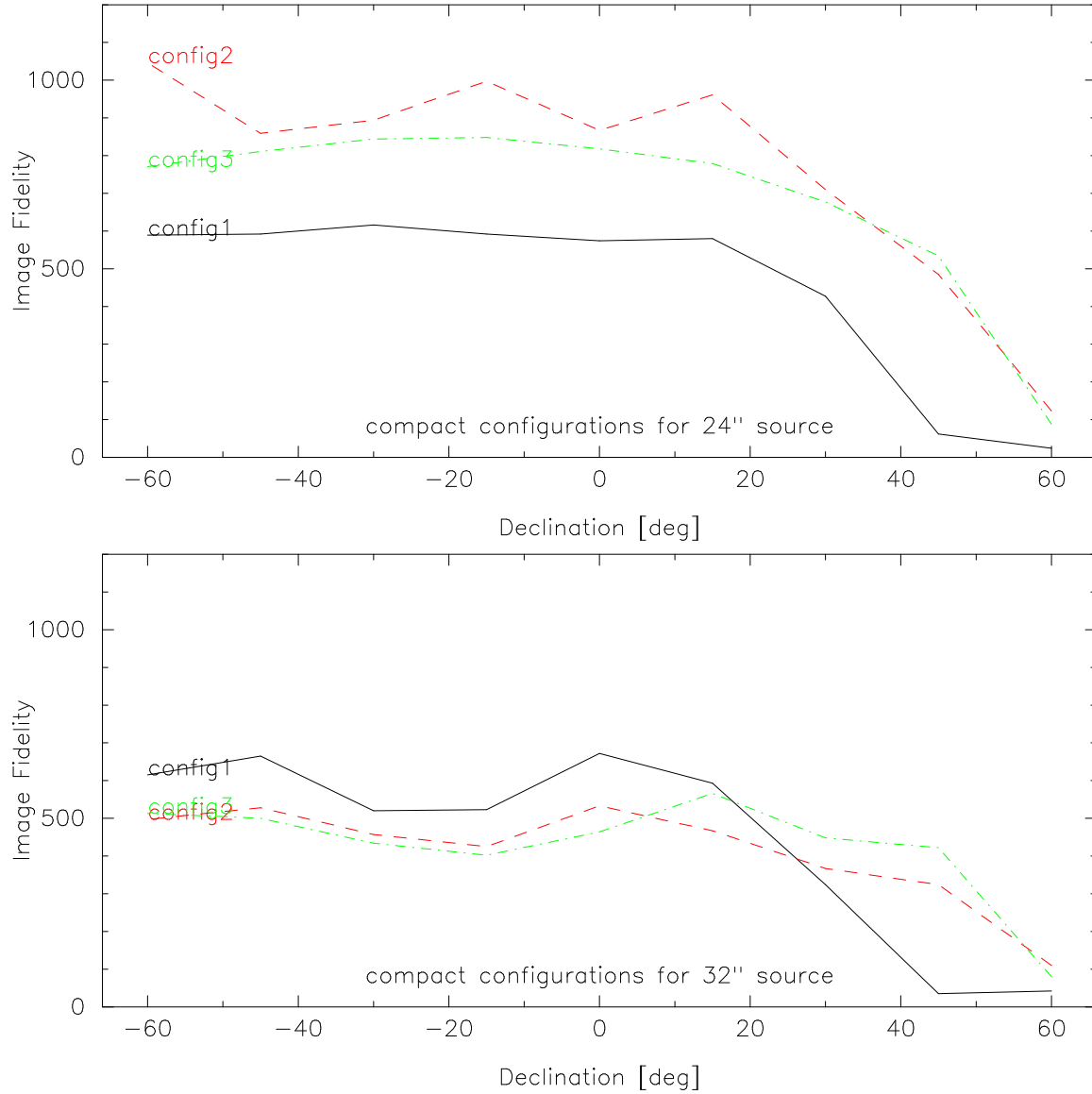


Fig. 3.— Image fidelity for the original compact configurations: config1 [solid black line], config2 [dashed red line], config3 [dotted green line]

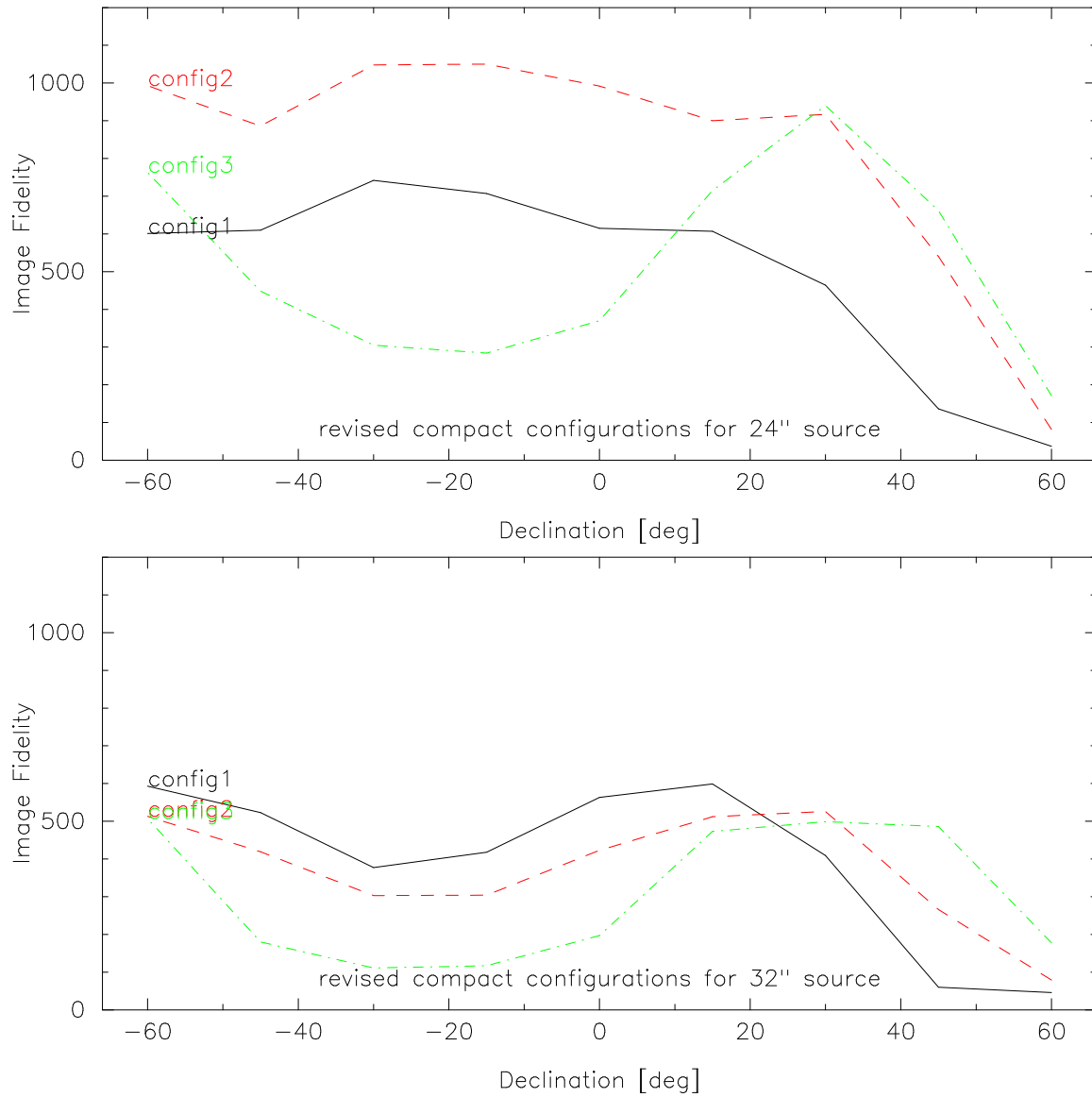


Fig. 4.— Image fidelity for the revised compact configurations: config1 [solid black line], config2 [dashed red line], config3 [dotted green line]

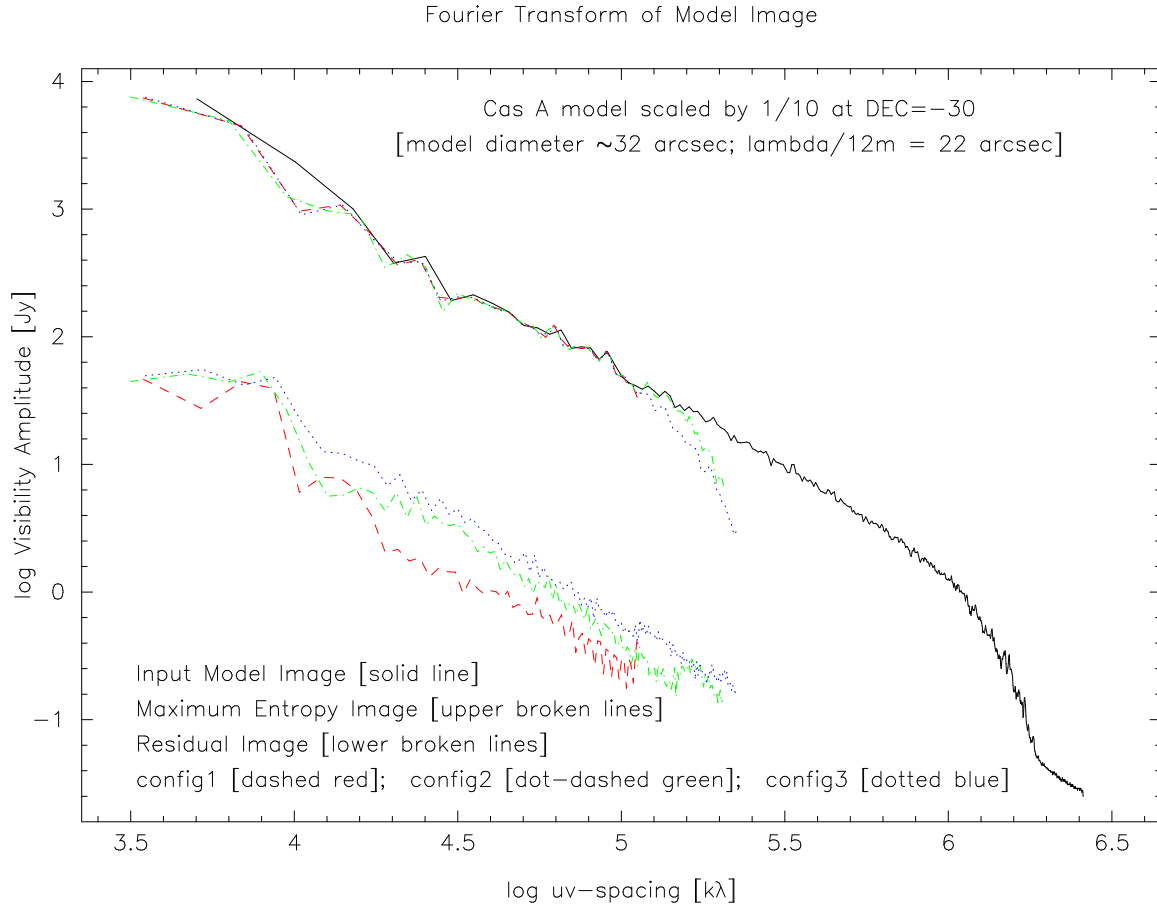


Fig. 5.— Radial distribution for Fourier Transform of Cas A model scaled by 1/10 at DEC=-30, and mosaiced images using original 3 compact configurations

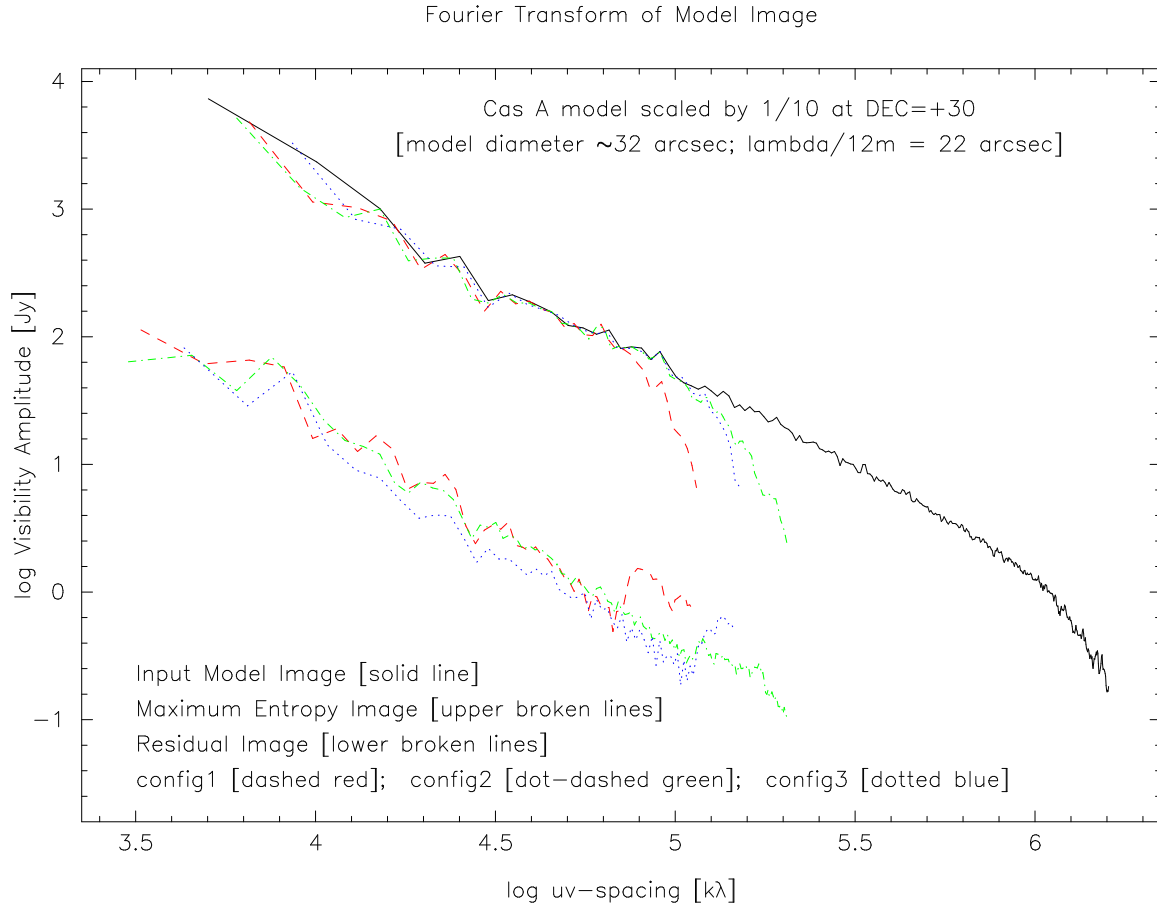


Fig. 6.— Radial distribution for Fourier Transform of Cas A model scaled by 1/10 at DEC=+30, and mosaiced images using original 3 compact configurations

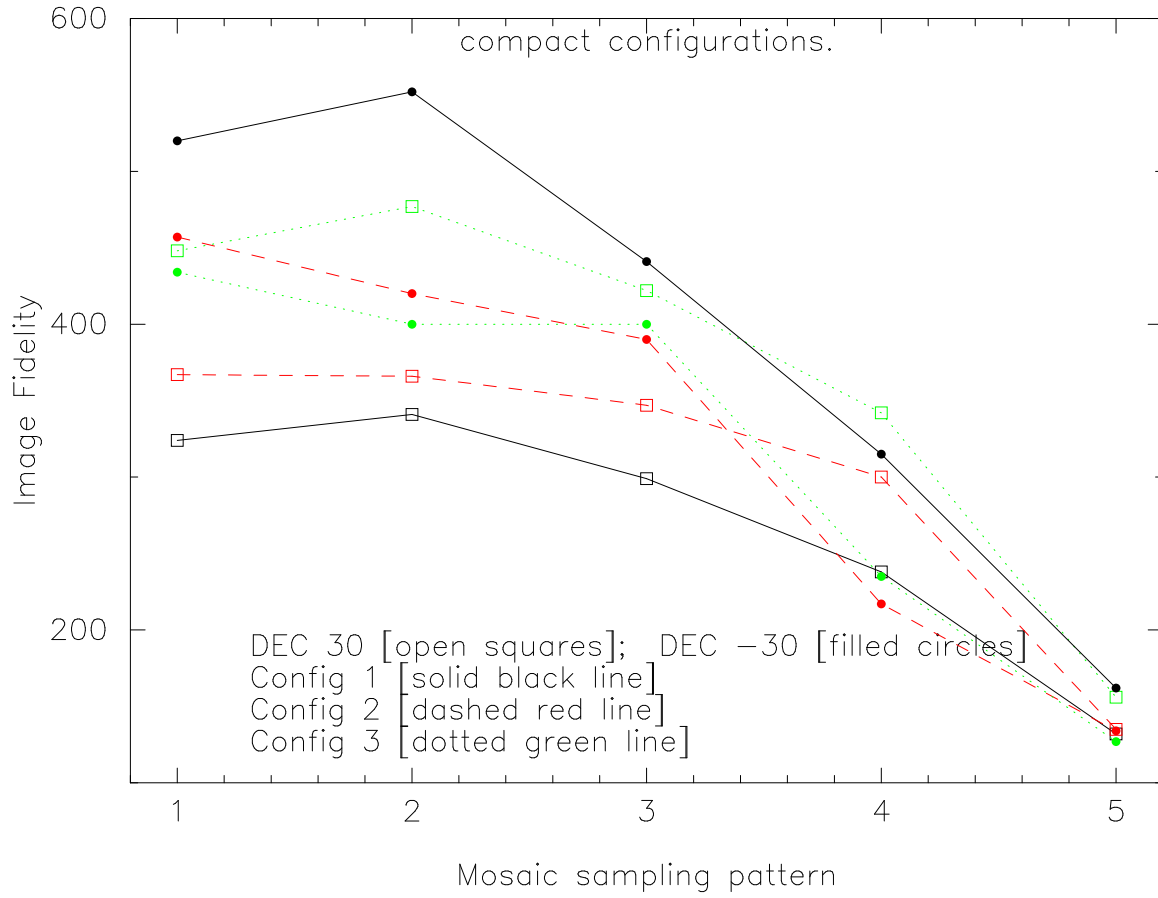


Fig. 7.— Image fidelity degradation with poorer pointing sampling for mosaiced images using the original 3 compact configurations

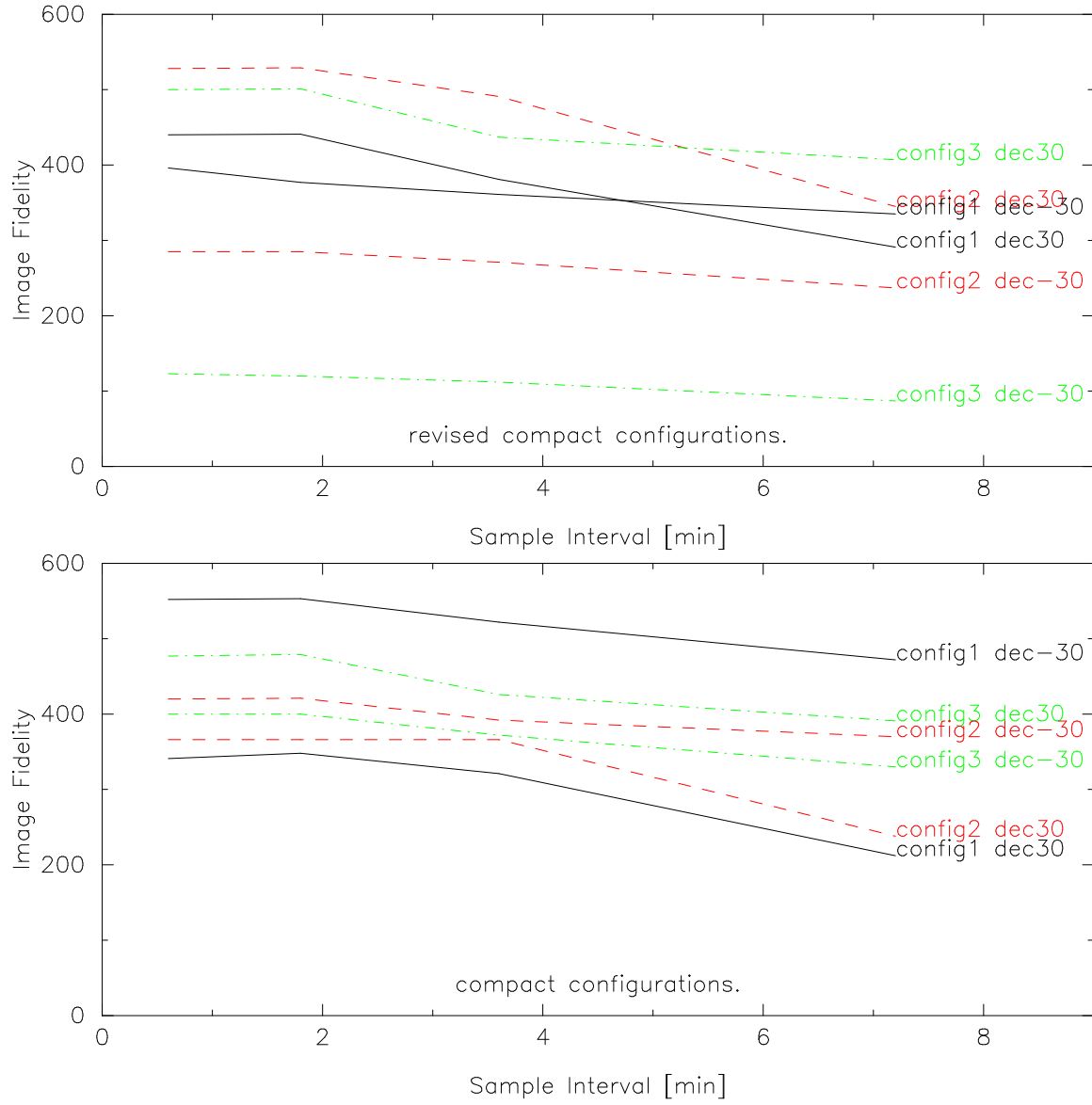


Fig. 8.— Image fidelity degradation with uv sample interval